High-Resolution NMR Studies of Chimeric DNA-RNA-DNA Duplexes, Heteronomous Base Pairing, and Continuous Base Stacking at Junctions†

Shan-Ho Chou,‡,§ Peter Flynn,‖ Andrew Wang,§ and Brian Reid*,§,‖

Departments of Biochemistry and Chemistry, University of Washington, Seattle, Washington 98195, and Howard Hughes Medical Institute, Seattle, Washington 98195

Received October 22, 1990; Revised Manuscript Received February 22, 1991

ABSTRACT: Two symmetrical DNA-RNA-DNA duplex chimeras, d(CGCG)r(AAUU)d(CGCG) (designated rAAUU) and d(CGCG)r(UAUA)d(CGCG) (designated rUAUA), and a nonsymmetrical chimeric duplex, d(CGTT)r(AUAA)d(TGCG)/d(CGCA)r(UUAU)d(AACG) (designated rAUAA), as well as their pure DNA analogues, containing dU instead of T, have been synthesized by solid-phase phosphoramidite methods and studied by high-resolution NMR techniques. The 1D imino proton NOE spectra of these d-r-d chimeras indicate normal Watson-Crick hydrogen bonding and base stacking at the junction region. Preliminary qualitative NOESY, COSY, and chemical shift data suggest that the internal RNA segment contains C3′-endo (A-type) sugar conformations except for the first RNA residues (position 5 and 17) following the 3′ end of the DNA block, which, unlike the other six ribonucleotides, exhibit detectable H1′-H2′ J coupling. The nucleosides of the two flanking DNA segments appear to adopt a fairly normal C2′-endo B-DNA conformation except at the junction with the RNA blocks (residues 4 and 16), where the last DNA residue appears to adopt an intermediate sugar conformation. The DNA-RNA junction residues exhibit quite different COSY, chemical shift, and NOE behavior, but these effects do not appear to propagate into the DNA or RNA segments. The circular dichroism spectra of these d-r-d chimeras also display a mixture of characteristic A-type and B-type absorption bands. The data indicate that A-type and B-type conformations can coexist in a single short continuous nucleic acid duplex, but our results differ somewhat from previous theoretical model studies.

The ability of double-helical DNA to exist in various conformations separated by relatively low energy barriers is now well recognized. Three major DNA forms, namely A-type, B-type, and left-handed Z-type, have been well documented both in fibers (Arnott et al., 1972, 1980) and in the crystal state (Wang et al., 1981, 1982; Dickerson & Drew, 1981; McCall et al., 1985, 1986; Shakked et al., 1983; Haran et al., 1987; Nelson et al., 1987). It is theoretically possible for two different DNA forms to coexist in a single continuous double helix. Arnott et al. (1983) were able to construct models of B-DNA embedded within a patch of Z-DNA as well as of B-DNA embedded within a patch of A-DNA, with only one base pair adopting a different conformation; both of these models were found to involve bending or kinking at the junction region. Subsequently, a B-Z junction has been observed in both natural DNA (Rich et al., 1984) and synthetic DNA oligomers (Sheardy, 1988; Adam et al., 1988), and a cell protein capable of binding to Z-DNA has also been reported (Leith et al., 1988). The possibility of a B-DNA/A-DNA junction in vivo was suggested by Rhodes and Klug (1986), who proposed that the DNA-binding site for transcriptional factor IIIA (TFIIIA) in the *Xenopus* 5S RNA gene region has an A-like structure on the basis of the observation that TFIIIA can bind to its target site in the double-stranded DNA structural gene as well as to the RNA transcript. On the basis of Raman spectroscopic studies of synthetic DNA oligomers in the solid state and in solution (Peticolas et al., 1988; Wang et al., 1987), this sequence contains strong determinants for potentially forming an A-form structure in solution. The concept of regulating DNA transcription and replication by DNA conformational changes is a relatively new idea that is largely unexplored, and this persuaded us to attempt to study the structure of B-A junctions in solution by 2D NMR methods. Previous attempts by us and others (Aboul-ela et al., 1988) to produce local segments of A-structure in pure DNA duplexes were unsuccessful, leading only to B-form duplexes; although the octamer d(GGTATACC) was found to crystallize in the A-form (Shakked et al., 1983), it was found to exist in longer duplexes, or even as the octamer alone (Reid et al., 1983), as a B-form duplex in solution. On the basis of a low-resolution 1D NMR study of dG_n:rC_{11}dC_{16} in H_2O solution (Selsing et al., 1978), Arnott et al. (1983) modeled a B-A junction and suggested that A and B conformations might coexist in a single continuous double helix. Some NMR data on d(CG)r(CG)d(CG) were reported by Haasnoot et al. (1983), but the spectra were not resolved enough to provide sufficient detail for reconstructing the junction conformation.

We have previously carried out extensive studies on the conformation of DNA using 2D NMR methods combined with distance geometry (Hare et al., 1983; Chou et al., 1983; Wemmer et al., 1984; Hare & Reid, 1986; Reid, 1987; Nerdal et al., 1989; Banks et al., 1989). Despite the absence of distal tertiary constraints in DNA, local nearest neighbor constraints still yield a wealth of detailed structural information. More recently, we have also carried out the synthesis of large amounts of specific oligoribonucleotide sequences using the TBDMS method of Ogilvie and co-workers to protect the 2′-OH (Ogilvie et al., 1988), and we are now able to synthesize up to 30 mg of short RNA duplexes or DNA/RNA hybrid oligomers for 2D NMR studies (Chou et al., 1989a,b). Our

† We gratefully acknowledge the support of NIH Grant GM 42896 from the U.S. Public Health Service.

* To whom correspondence should be addressed.
‡ Howard Hughes Medical Institute.
§ Department of Biochemistry, University of Washington.
‖ Department of Chemistry, University of Washington.

0006-2960/91/0430-5248$02.50/0

previous studies on r:r duplexes showed them to be in the A-type conformation (Chou et al., 1989a), whereas the corresponding d:d sequences invariably adopted a B-type structure (Hare et al., 1983; Wemmer et al., 1985). Because the ribonucleoside and deoxyribonucleoside phosphoramidite chemistries are completely compatible, we decided to covalently incorporate an RNA fragment into a DNA sequence with the goal of creating an A–B and a B–A junction in a single duplex. We therefore synthesized three chimeric dodecamers containing four central r:r base pairs surrounded by four d:d base pairs on each side for subsequent NMR studies. Each block of DNA or RNA is almost a half turn of the double helix, and the chimera contains potential A–B (RNA–DNA) and B–A (DNA–RNA) junctions.

Materials and Methods

The procedure for rapid and efficient solid-phase RNA synthesis using 5′-DMT-3′-*N*,*N*-diisopropylmethoxyphosphoramidites protected at the 2′-OH with a *t*-butyldimethylsilyl (TBDMS) group has been described previously (Ogilvie et al., 1988; Chou et al., 1989a); 10-μmol syntheses were carried out on an automated DNA synthesizer (Applied Biosystems model 380B) with the appropriate ribonucleoside phosphoramidites in the 5th, 6th, 7th, and 8th cycles. After heating at 55 °C overnight, the TBDMS protection group was removed by 2 mL of tetrabutylammonium fluoride (1 M solution in THF) at room temperature for 4 h, and the TBAF was removed by passage through a sodium form ion-exchange column. The sample was then chromatographed on a hydroxyapatite column with a phosphate gradient and finally desalted by passage through a Sephadex G-25 column eluted with H_2O.

NMR Spectroscopy. All NMR experiments were carried out at 31 °C on a Bruker WM-500 NMR spectrometer unless otherwise noted. Samples typically contained 15–20 mg of duplex dissolved in 0.4 mL of 10 mM sodium phosphate buffer, pH 7.0, containing 0.2 M NaCl. Exchangeable proton spectra were obtained by using a Redfield 214 solvent-suppression pulse sequence (Redfield, 1978) with the carrier frequency set at approximately 11.7 ppm and a total pulse length of 275 μs. NOE difference spectra were collected by coaveraging 16 scans with applied radio-frequency (rf) irradiation at a desired resonance position and then subtracting that sum from an equal number of scans with the rf placed off-resonance; a total of 3200 scans were accumulated. Absolute magnitude COSY data were collected by using 1024 complex points in t_2 and 400 t_1 points. NOESY spectra with a mixing time of 180 ms (randomly varied by ±10% to suppress zero-quantum coherence) were acquired in the phase-sensitive mode (States et al., 1982) by using 1024 complex points in t_2 and 400 pairs of real and imaginary t_1 experiments; 32 scans were collected per t_1 experiment with a relaxation delay of 2 s between scans. The COSY and NOESY data were processed with the FTNMR program (Hare Research, Woodinville, WA). The COSY data were apodized by using an unshifted sine-bell function. NOESY data were apodized with a skewed phase-shifted sine-bell function. Noise ridges in the t_1 dimension were attenuated by multiplying the first row by one-half prior to transformation (Otting et al., 1986).

Results

In order to prevent ambiguity in such terms as "interstrand NOEs to the following base pair", in the following discussion, we have adopted the same notation as in our previous paper (Chou et al., 1989a); that is, intrastrand NOEs are designated as *n* to *n* − 1 or *n* + 1, where *n* − 1 precedes *n*, i.e., is 5′ to *n* and interstrand NOEs are designated as *n* to *m* or *n* to *m* + 1, where *m* is paired to *n* and *m* + 1 follows *m*, i.e., is 3′ to *m*. Thus *n* − 1 and *m* + 1 are complementary base pairs as are *n* + 1 and *m* − 1.

One-Dimensional Imino Proton Studies. The 1D imino proton spectrum of rAAUU at 31 °C, together with some of the imino proton to imino proton NOEs, is presented in the supplementary material. Five well-resolved low-field resonances, accounting for five imino protons in this symmetrical dodecamer, are observed; the terminal imino resonance exchanges too fast to be observed at this temperature. The imino protons were assigned by using previously published nearest neighbor NOE procedures (Chou et al., 1983, 1989a). However, it is worth noting that the imino proton NOE pattern is nonreciprocal (i.e., U7 to U8 is weaker than U8 to U7 and G4 to U8 is weaker than U8 to G4) and some of the imino-to-imino proton NOEs, especially in the central RNA section, are very weak and only marginally reliable for assignment purpose. The 7U and 8U imino protons were therefore assigned from the A H2 resonances of the complementary strand that can be reliably assigned from the strong (*n*) A H2 to (*n* + 1) H1′ and (*n*) A H2 to (*m* + 1) H1′ NOEs in the RNA portion of the molecule (Chou et al., 1989a). The nonreciprocal nature of the imino proton NOEs is even more pronounced in the case of the nonsymmetrical rAUAA duplex shown in Figure 1, where eight well-resolved low-field peaks accounting for the ten internal imino protons are clearly seen. When the 17U imino proton is irradiated, a strong NOE to the 9T imino proton is observed (Figure 1D), but when the 9T imino proton is irradiated, no NOE back to the 17U imino proton can be detected (Figure 1C). A similar phenomenon is also observed for the 4T and 20U pair (Figure 1, spectra E and C). This nonreciprocal NOE pattern at the junction region of chimeric duplexes is consistently one directional, i.e., the RNA imino to DNA imino NOE is readily detectable but the DNA imino to RNA imino NOE is not. We have not investigated this observation further and do not have a definitive explanation of the phenomenon. However, the results indicate the occurrence of normal Watson–Crick base-pair hydrogen bonding and continuous base-pair stacking at the junction region and are consistent with increased solvent exchange of the RNA base pair at the junction. Evidence for a unique structure with altered base stacking at the RNA interface comes from a comparison of the U8 N3H resonance in rAAUU and in the dAAUU pure DNA duplex containing dU in positions 7 and 8, as shown in the supplementary material. In rAAUU the U8 and U7 imino protons exchange chemical shifts compared to dAAUU, with U8 moving upfield from 13.75 ppm in dAAUU to 13.4 ppm in rAAUU. In both duplexes, U8 is one of the most labile imino resonances, broadening at 54 °C slightly before G2 in rAAUU and slightly after G2 in dAAUU (see the supplementary material).

2D NMR Studies of Nonexchangeable Protons. The COSY spectra of rAAUU and rUAUA also indicate structural peculiarities at the junctions; the spectra are presented in the supplementary material. In rAAUU the H5 of 7U is markedly upfield shifted into the DNA H3′ region at 4.75 ppm. Compared to the pure DNA dAAUU dodecamer of the same sequence or the DNA analogue containing thymine (Hare et al., 1983), the H6 of 9C at the junction region has shifted downfield by 0.26 ppm while the H6 resonances of 1C, 11C, and 3C are virtually unchanged. In the RNA H1′ to H2′ region most of the ribose sugars show no 1′H–2′H coupling, indicating a C3′-endo A-type conformation with a H1′–H2′ dihedral angle close to 90°, but the junction residue 5A in

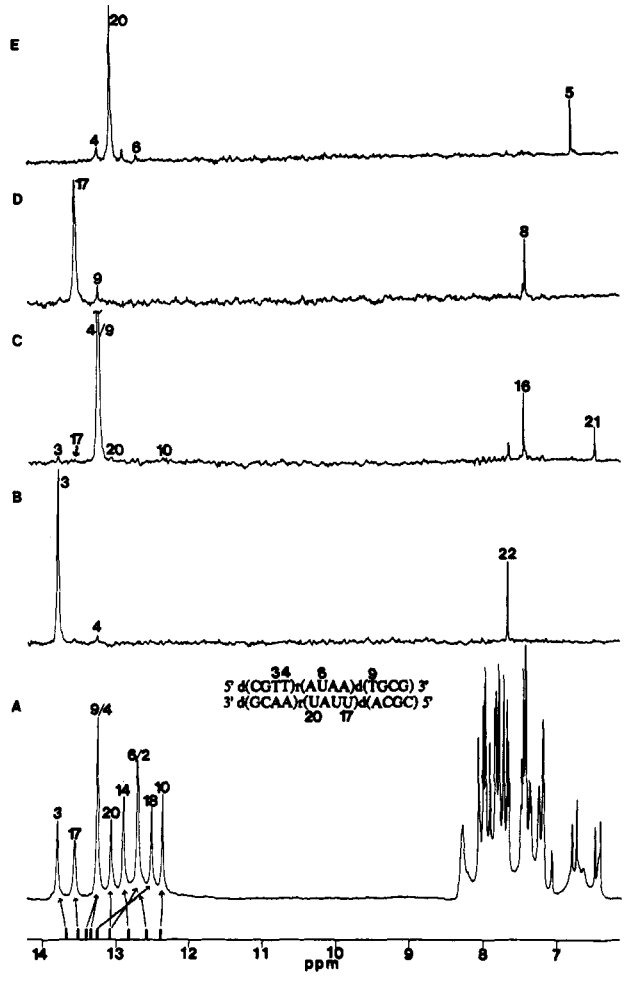

FIGURE 1: One-dimensional imino proton spectrum (bottom) and imino NOEs for the duplex rAUAA at 31 °C. The chemical shifts for the pure DNA duplex of the same sequence under the same experimental conditions are shown as solid bars along the abscissa for comparison. The imino protons of 18U and 6U have moved upfield dramatically into the GC imino proton region, while the imino protons of 17U and 20U have moved downfield compared to DNA.

rAAUU exhibits readily observable 1′H–2′H *J* coupling. In rUAUA, as was the case in rAAUU, the H6 of 9C at the junction region also shifts downfield compared to the pure DNA analogues, although to a lesser extent (0.1 ppm), and the H6 resonances of 1C, 11C, and 3C remain largely unchanged. In the RNA H1′ to H2″/H2′ region, again only the first ribonucleotide following the DNA block (in this case 5U) shows detectable 1′H–2′H *J* coupling. The expanded 1′H–2′H/2″H deoxyribonucleoside region of the COSY spectrum of rUAUA is shown in Figure 2; 9C is found to possess almost the same pattern (similar splitting and similar chemical shift difference between the downfield H2″ and the upfield H2′) as does 3C or 11C. However, 4G is *markedly different* in that the 2′H appears slightly *downfield* of the 2″H and 4G also shows a scalar coupling pattern more similar to the terminal 12G than to 10G. As in all other DNA duplexes, the 3′-terminal G12 is always abnormal in that its 2′H is downfield rather than upfield of the 2″H, indicating a different sugar pucker (or multiple conformations) for the 3′-terminal residue. Similar results were also obtained for the r(AAUU) duplex. The COSY spectra of both rAAUU and rUAUA clearly indicate nonsymmetrical sugar conformations for base pairs at the junction region; that is, the last DNA nucleotide at position 4 changes its sugar ring conformation, while its complementary nucleotide, residue 9, retains its original C2′-endo-like con-

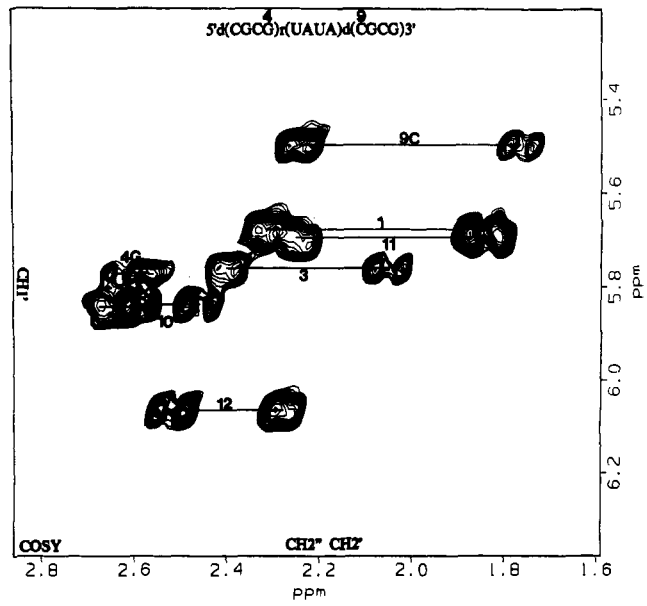

FIGURE 2: Expanded H1′ to H2′ region in the COSY spectrum of rUAUA. The junction nucleotide 4G is atypical in that the H2″/H2′ resonances are almost overlapped with H2′ slightly downfield of H2″ (as is the case for 12G). Residue 9C, following the RNA block, shows the normal coupling and H2″/H2′ chemical shift difference seen for the other deoxycytidines.

formation. Furthermore, the first RNA nucleotide at position 5 has a non-RNA-type sugar conformation, while its complementary residue 8 retains its C3′-endo-like conformation. At the junction region, it would appear that the last DNA pair and the first RNA pair both involve complementary Watson–Crick base pairing between nucleotides that are in *dissimilar conformations*.

Partial contour plots of the NOESY spectra of rAAUU and rUAUA are presented in Figure 3 panels A and B, respectively. Sequential assignment of the DNA base and sugar protons was accomplished according to previously published methods (Hare et al., 1983; Scheek et al., 1983; Feigon et al., 1983). The RNA assignments were made by using more recently published strategies devised for oligoribonucleotides (Chou et al., 1989a). The lack of H1′–H2′ coupling makes the H2′ protons somewhat more difficult to assign in RNA, but these assignments are facilitated by moderate-strength pyrimidine H5 to (n – 1) H2′ NOEs and strong H6/H8 to (n – 1) H2′ NOEs, as well as by the fact that the intraresidue H1′ to H2′ NOEs are always stronger than the intraresidue H1′ to H3′ and H1′to H4′ NOEs. Thus the base to (n – 1) H2′ and (n – 1) H1′ assignments are corroborated by (n – 1) H1′ to (n – 1) H2′ NOEs. One such example of an RNA H2′ assignment is shown in Figure 3A, and its NOE network is connected by solid lines. The 7U H6 cross peaks to 7U H5 and 6A H2′, together with the 6A H2′ cross peak to the known 6A H1′ resonance (see Figure 4A) and the 7U H5 to 6A H2′ cross peak, clearly identify the 6A H2′ resonance. Similarly, the 9C H6 to 9C H5 and 8U H2′ connectivities clearly identify the 8U H2′ resonance position (shown as dotted lines in Figure 3A). The H1′ to H2′ NOEs of the RNA block and the H1′ to H3′/H4′ NOEs of the DNA block in rAAUU are enclosed in box **c** in Figure 3A. Four strong RNA H1′ to H2′ NOEs are identified in this way (7U, 8U, 6A, and 5A). The 5A H2′ is further corroborated by H1′–H2′ *J*-coupling in the COSY spectrum (see the supplementary material). In the DNA H1′ to H2″/H2′ region (box **d**), 9C shows the same H1′ to H2″/H2′ NOE pattern as do the other deoxycytidines (expansion not shown).

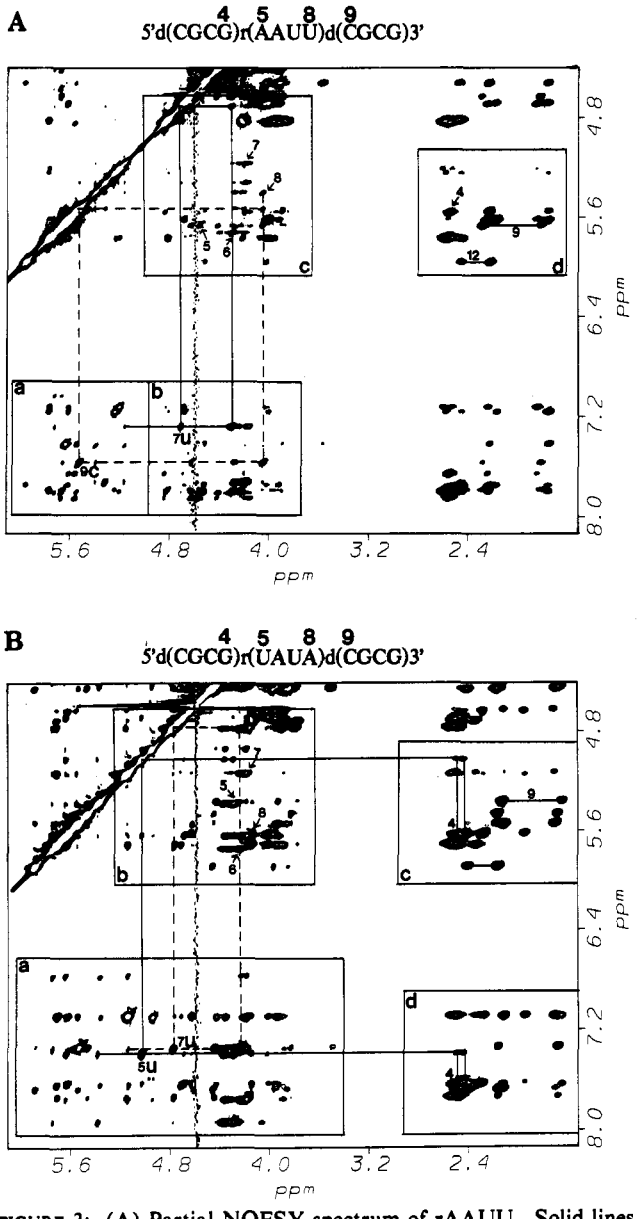

FIGURE 3: (A) Partial NOESY spectrum of rAAUU. Solid lines connect the NOE network H6(7) to H1′(7), H5(7), and H2′(6) as well as H2′(6) to H1′(6) and H5(7). Dotted lines connect the analogous 9C–8U network. The four strong H1′ to H2′ NOEs of the RNA strand are indicated by arrows in box **c**. The NOEs from H1′ to H2″/H2′ of 4G, 9C, and 12G are also labeled in box **d**. (B) Partial NOESY spectrum of rUAUA. The network of dashed lines connects the NOEs from 7U H5/H6 to 6A H1′/H2′, and the solid line network connects the NOEs from 5U H5/H6 to 4G H1′/H2′ and H2″. Four strong H1′ to H2′ NOEs of the RNA strand are labeled with arrows in box **b**. The NOEs of H1′ to H2″/H2′ of 4G and 9C are also labeled in box **c**.

The NOESY spectrum of rUAUA is shown in Figure 3B; four strong RNA H1′ to H2′ NOEs are well resolved and are enclosed in box **b**. As in the rAAUU case, we have connected 7U H6 cross peaks to 7U H5 and 6A H2′, as well as the 7U H5 to 6A H2′ cross peak, with dotted lines. The NOEs at the d–r junction, 5U H6 to 5U H5 and to 4G H2″/H2′, are now well resolved and are connected by solid lines (box **a** and **d**); the 5U H5 to 4G H2″/H2′ NOEs are shown in box **c**. The DNA H1′ to H2″/H2′ NOE region is enclosed in box **c** and again reveals that 9C at the r–d junction exhibits a NOE pattern similar to the other deoxycytidines. The NOE pattern for 4G, on the other hand, is *more similar to 12G* than to other guanosines in that the H1′ to H2′ NOE appears to be just as strong as the H1′ to H2″ NOE (expanded region not shown).

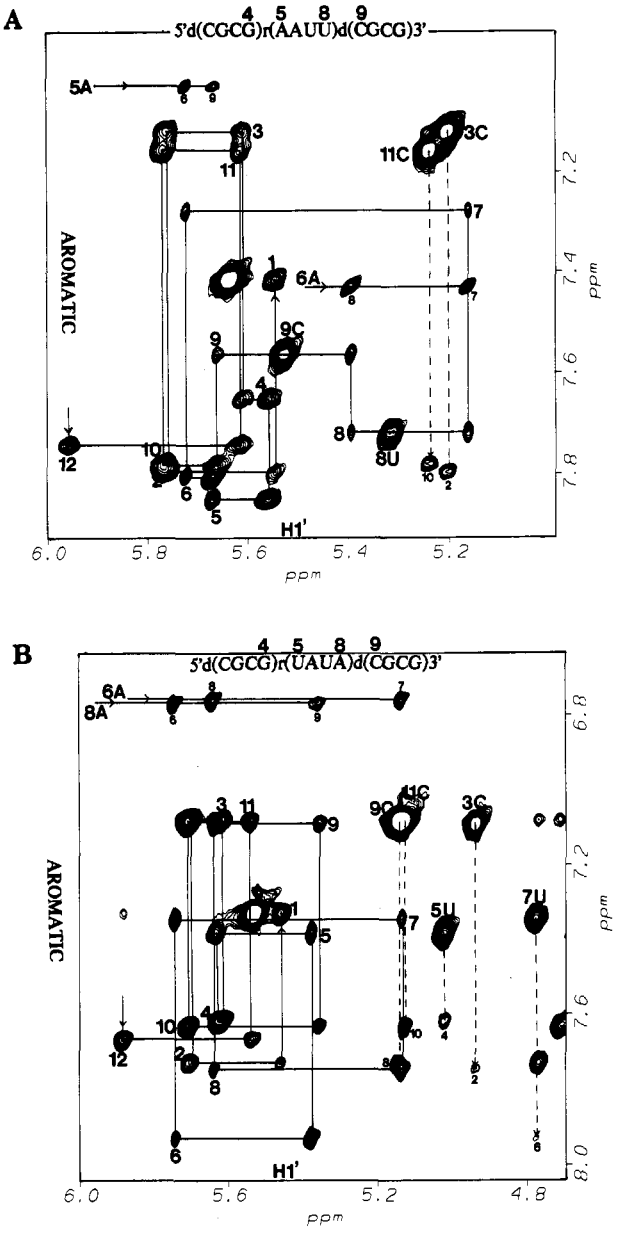

FIGURE 4: (A) Expanded NOESY spectrum of the H8/H6/H2 to H1′ proton region in rAAUU. Sequential (*n*) H8/H6 to (*n*) and (*n* − 1) H1′ peaks are connected by solid lines with the (*n*) H8/H6 to (*n*) H1′ designated by the residue number. The H5 cross peaks to (*n*) H6 and (*n* − 1) H6/H8 in the DNA segments are connected by vertical dashed lines and are not observed for C9 and U8. The weaker peaks in the RNA block are due to partial saturation of the RNA protons (long T_1) during the 2-s relaxation delay. (B) Expanded NOESY spectrum of the H8/H6/H2 to H1′ proton region in rUAUA. The six strong H5–H6 peaks are clearly seen and are connected to the (*n* − 1) H6/H8 resonances by vertical dashed lines. The upper horizontal bars connect the inter- and intrastrand AH2 to H1′ NOEs.

The expanded H6/H8/H2 to H1′ NOESY region of rAAUU is shown in Figure 4A. The standard inter- and intraresidue H6/H8 to H1′ NOE connectivities can be traced all the way down the chain, including the junction region area. It is interesting to note that most of the H6/H8 to (*n*) H1′ and H6/H8 to (*n* − 1) H1′ NOEs in the central RNA block are weaker than those in the DNA blocks. However, this observation is merely the result of partially saturating the RNA protons that have longer T_1 values than the corresponding DNA protons (Wang et al., submitted for publication) and exceed the 2-s relaxation delay used in acquiring the data; it does not necessarily reflect correspondingly greater

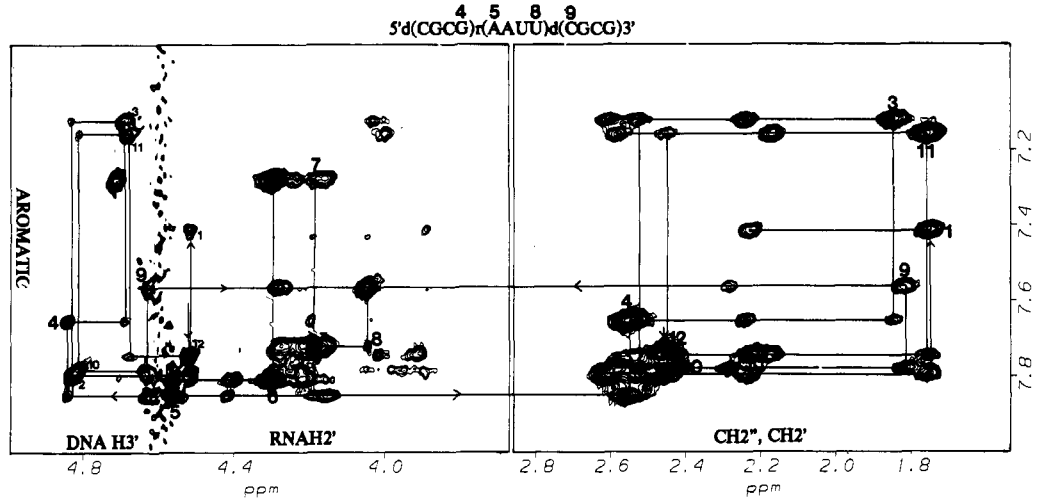

FIGURE 5: Expanded H6/H8 to DNA H3′ and RNA H2′, and H6/H8 to DNA H2′/H2″ regions of the NOESY spectrum of rAAUU. Starting from the H6/H8 to DNA H2′/H2″ region, sequential NOE connectivities jump to the RNA H2′ region (9C H6 to 8U H2′) and then back to the DNA region (5A H8 to 4G H3′/H2′). The strong 9C H6 to 8U H2′ NOE is evident in the left panel. Two other strong (*n*) H6/H8 to (*n* − 1) H2′ NOEs in the RNA H2′ region, characteristic of the C3′-endo conformation, are also seen.

H8/H6–H1′ distances in the RNA segment. Also, the interstrand 5A H2 to 9C H1′ NOE at the junction region is also clearly detected (upper horizontal line in Figure 4A) as is the cross-strand 6A H2 to 8U H1′ NOE within the RNA block. The base to H1′ NOESY region of rUAUA is shown expanded in Figure 4B, and again the NOEs of the central RNA nucleotides are weaker, because of partial saturation, than those of the nucleotides in the two terminal DNA blocks. The inter- and intrastrand H2 to H1′ NOEs in the RNA blocks are obvious and are indicated by the two horizontal lines at the top of Figure 4B.

The expanded NOESY spectra of the base to DNA H3′/RNA H2′ and the base to DNA H2′/H2″ regions of r(AAUU) are shown in Figure 5. Sequential NOE connectivities can be traced through the DNA H3′/H2′ region (12G to 9C), then jump to the RNA H2′ region (8U to 5A), and then back again to the DNA H3′/H2′ region (4G to 1C). At the junctions, strong 9C H6 to 8U H2′ and 5A H8 to 4G H2′/H2″ NOEs and a weaker 5A H8 to 4G H3′ NOE are observed. In the base to DNA H2′/H2″ region on the right side, it can be clearly be seen that intraresidue (*n*) H6/H8 to (*n*) H2′ NOEs are much stronger than interresidue (*n*) H6/H8 to (*n* − 1) H2′ NOEs in the DNA segments (as expected for a B-type conformation), whereas in the RNA segments the interresidue (*n*) H6/H8 to (*n* − 1) H2′ NOEs are stronger than the intraresidue (*n*) H6/H8 to (*n*) H2′ NOEs (indicating A-type structure). Similar results were obtained for the r(UAUA) duplex. These two NOESY spectra, together with the COSY spectra, clearly indicate that the DNA segments have a B-type helix geometry with C2′-endo sugar conformations while the RNA segment has an A-type geometry with C3′-endo sugar conformations. Despite the change in helix geometry, the base–H1′ and base–H2′ sequential connectivities from residues 1 to 12 indicate that continuous base stacking is maintained at both junction regions.

The Nonsymmetrical r(AUAA) Duplex. The COSY spectrum of the nonsymmetrical rAUAA duplex is presented in Figure 6. In the RNA H1′ to H2′ region (box **b**), 5A and 17U both exhibit detectable H1′ to H2′ *J* couplings while the other six ribonucleotides do not, i.e., the first RNA residue following the DNA block on both strands takes on an altered conformation while the complementary ribonucleotides 8A and 20U remain in a normal C3′-endo conformation and show no scalar coupling in this region. In the H5 to H6 region (box

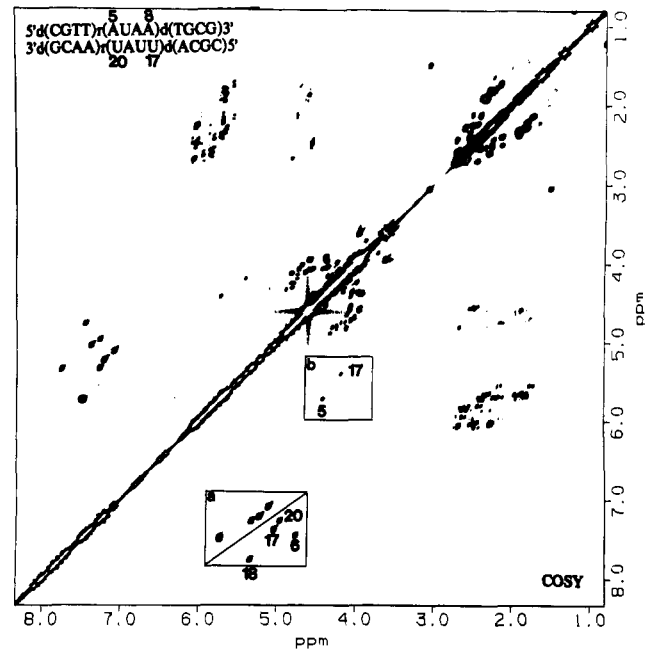

FIGURE 6: COSY spectrum of the nonsymmetrical rAUAA duplex. Both 5A and 17U are now seen to exhibit detectable *J* coupling, due to the asymmetry of the sequence. The DNA cytidine and RNA uridine H5 to H6 *J* couplings are enclosed in box **a** and separated by a diagonal line.

a), we detect nine strong peaks that fall on either side of a diagonal with the upper left half belong to the five DNA cytidines (1 and 13 are overlapped) and the lower right half belonging to the four RNA uracils. The cytidines of the DNA block show little chemical shift change when compared to the pure DNA analogue of the same sequence. In contrast, the RNA uridine H5–H6 cross peaks in the lower right half show dramatic chemical shift changes compared to the identical pure DNA analogue containing dU at positions 6, 17, 18, and 20. Figure 7, panels A and B, shows the H8/H6 to H1′, H2 to H1′, and H2 to H2 NOEs in the nonsymmetrical rAUAA chimera and the pure DNA dAUAA analogue. In the rAUAA chimeric duplex, results similar to those for the symmetrical rAAUU and rUAUA chimeras were observed. The H8/H6 to H1′ sequential connectivities could be traced for each strand separately, but the 21H8–20H1′ and 9H6–

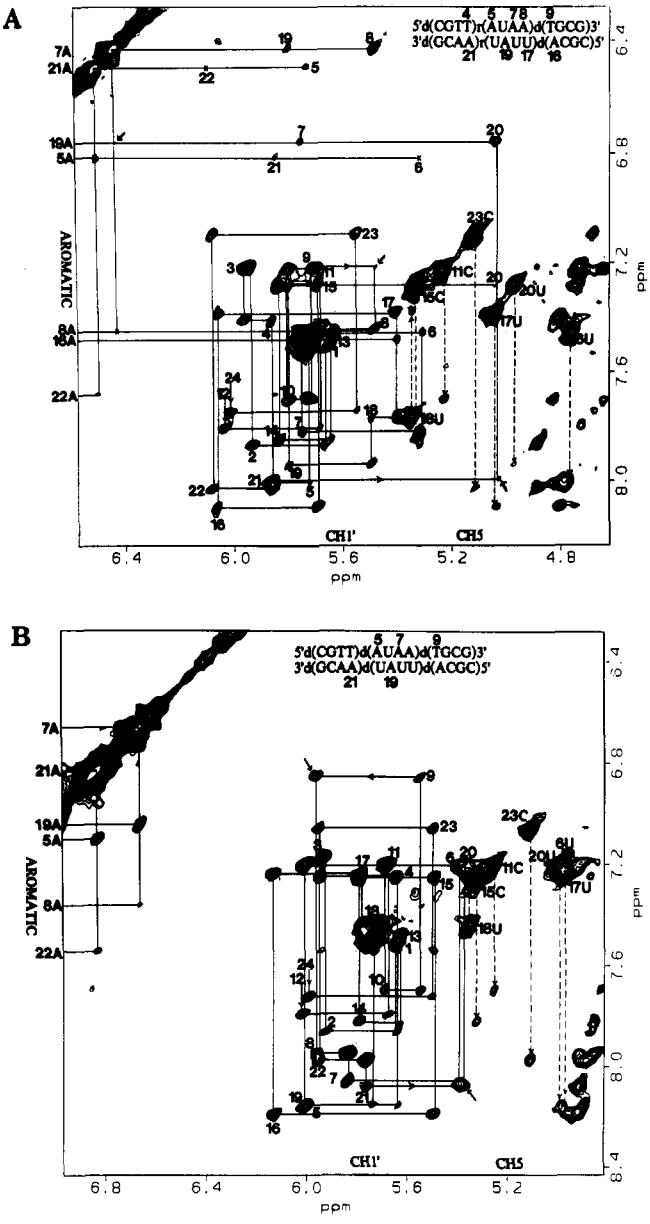

FIGURE 7: (A) Partial NOESY spectrum of the rAUAA duplex showing H8/H6–H1′ cross peaks, H2–H1′ cross peaks, and H2–H2 cross peaks. The vertical dashed lines indicate H6–H5 to $(n-1)$ H8/H6 connectivities. (B) Partial NOESY spectrum of the dAUAA pure DNA analogue of the rAUAA duplex. The sequential H8/H6 to H1′ connectivities are traced by a solid line, and the H6/H5 to $(n-1)$ H8/H6 connectivities are designated with vertical dashed lines. The H6–H5 cross peaks for U6, U17, U18, and U20 are markedly shifted from their positions in the rAUAA chimera (see Table III).

8H1′ NOEs at the r–d junctions are weak or absent (due mostly to the effects of partial relaxation and symmetrization of this spectrum). The 19AH2–7AH2 NOE typical of B-DNA is strong in the dAUAA pure DNA duplex but is extremely weak in the A-type central segment of rAUAA. Interestingly, the dA21H2–rA5H2 NOE across the d–r junction in rAUAA is of intermediate strength, i.e., weaker than the B-type dA21H2–dA5H2 NOE in dAUAA but stronger than the A-type rA19H2–rA7H2 in the center of rAUAA. In the interior of the rAUAA segment, strong (n) H2 to $(n+1)$ H1′ and $(m+1)$ H1′ NOEs characteristic of inclined A-type duplexes are observed, e.g., 7H2 to 8H1′ and 19H1′ as well as 19H2 to 20H1′ and 7H1′, which are not observed in the dAUAA duplex. However, at the d–r junction, 5AH2 exhibits an extremely weak $(n+1)$ NOE to 6H1′ and a modest $(m+1)$ cross-strand NOE to 21 H1′, and, similarly, 21AH2 exhibits a negligible $(n+1)$ NOE to 22H1′ and a medium $(m+1)$ cross-strand NOE to 5H1′ (Figure 7a), indicating a structure at the d–r junction that is neither A-type nor B-type. Unfortunately, at the r–d junction, the 8A and 16A H2 chemical shifts are in the H8/H6 chemical shift region, and the H2 NOEs to $(n+1)$ and $(m+1)$ H1′ resonances are not resolved.

Elsewhere in the NOESY spectrum of rAUAA (see the supplementary material), the H8/H6 to H3′ NOEs and the H8/H6 to H2′ NOEs can also be traced sequentially for each strand separately. During this process, we also noted strong 9TH6–8AH2′ and 21AH8–20UH2′ NOEs at the r–d junctions and strong 5AH8–4TH2′/H2″ and 17UH6–16AH2′/H2″ NOEs at the d–r junctions. The chemical shifts of the rAUAA chimeric duplex and the dAUAA DNA duplex are listed in Table III.

Discussion

The possibility of regulating gene activity by changes in DNA conformation is an intriguing one. TFIIIA binds to the 5S RNA transcript and Rhodes and Klug (1986) have proposed that the DNA-binding site for this protein in the *Xenopus* 5S RNA gene has an A-type rather than a B-type structure. The existence of kinks at A–B junctions might produce a repeating motif of a half-turn A-form and a half-turn B-form resulting in a loop structure as suggested by Selsing et al. (1979), which could have important biological functions. Although we were unable to produce segments of A-DNA in short pure DNA duplexes, in the present work we attempted to create internal A-duplex in B-duplex regions by inserting short RNA segments into a DNA duplex in order to create B–A and A–B junctions; in DNA the A-form and B-form double helices appear to have rather similar free energies (Broyde et al., 1975) and are most likely to coexist simultaneously. The present results clearly indicate that A-form and B-form duplexes can and do coexist in a single continuous double helix.

The DNA Segments of Chimeric Duplexes Assume a Normal B-Type Conformation. DNA has the ability to vary its helix geometry and sugar conformation under different conditions (Franklin & Gosling, 1953; Shakked et al., 1983; Sarma et al., 1986; Chou et al., 1989b), while RNA exists in the A-form under most conditions (Zimmerman & Pheiffer, 1981; Arnott et al., 1986; Chou et al., 1989a,b). It was therefore of interest to see if the central ribonucleotides in chimeric duplexes would influence the surrounding DNA, causing it to adopt the same conformation as RNA. On the basis of the following lines of evidence, we conclude that the DNA sections in d–r–d chimeras have a B-type structure and are not transformed into a different conformation, except at the junction base pair: (1) As shown in Figure 5, strong (n) H8/H6 to (n) H2′ NOEs and weak (n) H8/H6 to $(n-1)$ H2′ NOEs are observed for the deoxyribonucleotides; this is a very diagnostic characteristic of the B-type conformation (Hare et al., 1983; Reid et al., 1983; Haasnoot et al., 1984). (2) The coupling pattern of the H1′–H2″/H2′ protons of the DNA residues in the chimeras is similar to those in pure DNA sequences (Figure 2), which indicates a similar B-type conformation for these nucleotides; exceptions are the junction residues, which adopt an intermediate conformation and are perturbed by the interface. (3) The chemical shift values listed in Tables I, II, and III clearly indicate very little chemical shift change (<0.05 ppm in most cases) for all the nonexchangeable protons of the first two and last two base pairs in the DNA sections of the chimeric duplexes compared to the corresponding pure DNA duplexes. The DNA base pairs imme-

Table I: Proton Chemical Shifts in Chimeric Duplexes (DRD) and Pure DNA Duplexes (DDD) for the Sequence CGCGAAUUCGCG[a]

	C8H and C6H			C1′H			C5H			C3′H		
	d–d–d	d–r–d	Δ	d–d–d	d–r–d	Δ	d–d–d	d–r–d	Δ	d–d–d	d–r–d	Δ
1C	7.48	7.56	−0.08	5.62	5.67	−0.05	5.77	5.80	−0.03			
2G	7.82	7.87	−0.05	5.77	5.82	−0.05				4.86	4.87	−0.01
3G	7.14	7.19	−0.05	5.50	5.66	−0.16	5.26	5.27	−0.01	4.68	4.73	−0.05
4G	7.72	7.72	0.00	5.30	5.62	−0.32				4.87	4.88	−0.01
5A	7.98	7.90	0.08	5.84	5.72	0.12				4.94		
6A	7.96	7.85	0.11	5.97	5.78	0.19				4.83		
7U	7.17	7.33	−0.16	5.78	5.20	0.58	5.30	4.75	0.55	4.73		
8U	7.48	7.75	−0.27	6.02	5.44	0.58	5.31	5.36	−0.05	4.79		
9C	7.36	7.62	−0.26	5.54	5.62	−0.08	5.55	5.58	−0.03	4.77	4.67	0.10
10G	7.79	7.83	−0.04	5.74	5.82	−0.08				4.87	4.85	0.02
11C	7.21	7.22	−0.01	5.65	5.72	−0.07	5.32	5.28	0.04	4.70	4.72	−0.02
12G	7.81	7.81	0.00	6.02	6.02	0.00						

	C4′H			C2″H			C2′H		
	d–d–d	d–r–d	Δ	d–d–d	d–r–d	Δ	d–d–d	d–r–d	Δ
1C	3.95			2.28	2.29	−0.01	1.82	1.81	0.01
2G	4.23	4.26	−0.03	2.59	2.64	−0.05	2.54	2.57	−0.03
3C	4.00	4.07	−0.07	2.14	2.38	−0.24	1.68	1.91	−0.23
4G	4.19	4.24	−0.05	2.61	2.60	0.01	2.53	2.60	−0.07
5A	4.32			2.79			2.54	4.62	
6A	4.34			2.71			2.45	4.34	
7U	4.13			2.41			1.94	4.21	
8U	4.13			2.48			2.04	4.08	
9C	4.02	4.04	−0.02	2.28	2.32	−0.04	1.95	1.87	0.08
10G	4.24	4.24	0.00	2.58	2.60	−0.02	2.52	2.48	0.04
11C	4.04	4.06	−0.02	2.20	2.24	−0.04	1.78	1.81	−0.03
12G	4.04			2.28	2.25	0.03	2.50	2.50	0.00

[a] Values in the Δ column indicate differences in chemical shift for the chimera compared to pure DNA.

Table II: Proton Chemical Shifts in Chimeric Duplexes (DRD) and Pure DNA Duplexes (DDD) for the Sequence CGCGUAUACGCG[a]

	C8H and C6H			C1′H			C5H			C3′H		
	d–d–d	d–r–d	Δ	d–d–d	d–r–d	Δ	d–d–d	d–r–d	Δ	d–d–d	d–r–d	Δ
1C	7.54	7.54	0.00	5.70	5.67	0.003	5.81	5.78	0.03			
2G	7.87	7.87	0.00	5.83	5.84	−0.01				4.88	4.89	−0.01
3C	7.23	7.22	0.01	5.66	5.76	−0.10	5.30	5.07	0.23	4.73	4.74	−0.01
4G	7.81	7.75	0.06	5.81	5.78	0.03				4.90	4.80	0.10
5U	7.33	7.49	−0.16	5.70	5.50	0.20	5.12	5.14	−0.02	4.80		
6A	8.21	8.02	0.19	6.08	5.87	0.21				4.93		
7U	7.26	7.44	−0.18	5.52	5.25	0.27	5.03	4.89	0.14	4.77		
8A	8.15	7.89	0.26	6.08	5.76	0.32				4.92		
9C	7.14	7.22	−0.08	5.45	5.49	−0.04	5.17	5.29	−0.12	4.70	4.55	0.15
10G	7.76	7.76	0.00	5.77	5.84	−0.07				4.87	4.82	0.05
11C	7.23	7.22	0.01	5.69	5.72	−0.03	5.33	5.27	0.06	4.73	4.73	0.00
12G	7.82	7.81	0.01	6.07	6.02	0.05						

	C4′H			C2″H			C2′H		
	d–d–d	d–r–d	Δ	d–d–d	d–r–d	Δ	d–d–d	d–r–d	Δ
1C	3.99	3.96	0.03	2.33	2.30	0.03	1.88	1.82	0.06
2G	4.28	4.27	0.01	2.57	2.66	−0.99	2.59	2.59	0.00
3C	4.12	4.13	−0.01	2.34	2.39	−0.05	1.94	2.06	−0.12
4G	4.27	4.26	0.01	2.61	2.56	0.05	2.58	2.61	−0.03
5U	4.14			2.42			1.98	4.41	
6A	4.32			2.74			2.61	4.36	
7U	4.08			2.33			1.88	4.30	
8A	4.30			2.74			2.57	4.30	
9C	4.04	4.06	−0.02	2.19	2.23	−0.04	1.81	1.77	0.04
10G	4.24	4.24	0.00	2.60	2.60	0.00	2.50	2.45	0.05
11C	4.06	4.06	0.00	2.23	2.24	−0.01	1.82	1.83	−0.01
12G				2.28	2.26	0.02	2.54	2.52	0.02

[a] Values in the Δ column indicate differences in chemical shift for the chimera compared to pure DNA.

diately adjacent to the RNA block do exhibit significant chemical shift changes (up to 0.3 ppm depending on the sequence) that are to be expected since the chemical shifts of nucleic acid protons are predominantly determined by ring-current shifts from neighbors and nearest neighbors and hence are influenced by local structure.

RNA Nucleotides Maintain Their Normal A-Type Conformation. On the basis of the following evidence, we conclude that RNA nucleotides in d–r–d chimeras are in a typical A-type conformation, except those at the junction region: (1) As shown in Figure 5, strong (n) H8/H6 to ($n-1$) H2′ NOEs and weak (n) H8/H6 to (n) H2′ NOEs are observed for the RNA nucleotides; this is a characteristic of the A-type C3′ endo conformation (Reid et al., 1983; Haasnoot et al., 1984; Chou et al., 1989a). (2) In the 1D NMR proton spectrum, the H1′ resonances of the RNA residues (except positions 5 and 17) appear as very narrow singlets, almost as sharp as the A H2 peaks (data not shown). Furthermore, in the H1′ to

Table III: Proton Chemical Shifts in Chimeric Duplexes (DRD) and Pure DNA Duplexes (DDD) for the Sequence CGTTAUAATGCG + CGCAUUAUAACG[a]

	C8H and C6H			C1′H			C5H			C3′H		
	d-d-d	d-r-d	Δ	d-d-d	d-r-d	Δ	d-d-d	d-r-d	Δ	d-d-d	d-r-d	Δ
1C	7.52	7.50	0.02	5.64	5.67	−0.03	5.73	5.73	0.00			
2G	7.87	7.85	0.02	5.92	5.93	−0.01				4.88	4.88	0.00
3T	7.18	7.22	−0.04	5.94	5.97	−0.03				4.74	4.74	0.00
4T	7.26	7.40	−0.14	5.64	5.86	−0.22					4.82	
5A	8.17	8.02	0.15	6.00	5.72	0.28				4.98		
6U	7.22	7.45	−0.23	5.38	5.76	−0.38	4.98	4.77	0.21	4.72		
7A	8.08	7.82	0.26	5.82	5.31	0.51				4.90		
8A	7.95	7.45	0.50	5.95	5.48	0.47				4.84		
9T	6.85	7.22	−0.37	5.55	5.72	−0.17				4.69	4.64	0.05
10G	7.71	7.70	0.01	5.67	5.80	−0.13				4.84	4.83	0.01
11C	7.22	7.23	−0.01	5.66	5.67	−0.01	5.25	5.22	0.03	4.69	4.73	−0.04
12G	7.80	7.81	−0.01	6.01	6.04	−0.03				4.54	4.54	0.00
13C	7.48	7.48	0.00	5.62	5.64	−0.02	5.73	5.73	0.00			
14G	7.84	7.86	−0.02	5.79	5.83	−0.04				4.86	4.88	−0.02
15C	7.26	7.28	−0.02	5.49	5.68	−0.19	5.32	5.34	−0.02	4.72	4.74	−0.02
16A	8.22	8.10	0.12	6.14	6.07	0.07				4.92	4.80	0.12
17U	7.26	7.38	−0.12	5.78	5.41	0.37	4.95	5.03	−0.08	4.73		
18U	7.48	7.77	−0.29	5.73	5.50	0.23	5.34	5.35	−0.01			
19A	8.17	7.94	0.23	6.01	5.80	0.21				4.90		
20U	7.22	7.28	−0.06	5.37	5.85	−0.48	4.99	4.97	0.02	4.72		
21A	8.09	8.00	0.09	5.76	5.86	−0.10				4.92	4.78	0.14
22A	7.99	8.03	−0.04	5.94	6.09	−0.15				4.88	4.88	0.00
23C	7.05	7.10	−0.05	5.49	5.55	−0.06	5.10	5.12	−0.02	4.72	4.68	0.04
24G	7.73	7.74	−0.01	5.98	6.02	−0.04				4.50	4.54	−0.04

	C4′H			C2″H			C2′H		
	d-d-d	d-r-d	Δ	d-d-d	d-r-d	Δ	d-d-d	d-r-d	Δ
1C	3.95	3.96		2.32	2.32	0.00	1.91	1.92	−0.01
2G	4.28	4.28	0.00	2.72	2.72	0.00	2.58	2.61	−0.03
3T	4.13	4.17	−0.04	2.44	2.52	−0.08	1.98	2.14	−0.16
4T	4.03	4.11	−0.08	2.37			1.98		
5A	4.28			2.69			2.56	4.43	
6U	4.03			2.24			1.83	4.38	
7A	4.10			2.78			2.58	4.25	
8A	4.00			2.73			2.38	4.18	
9T	3.98	4.11	−0.13	2.18	2.38	−0.20	1.74	1.92	−0.18
10G	4.22	4.25	−0.03	2.52	2.55	−0.03	2.45	2.41	0.04
11C	4.04	4.08	−0.04	2.21	2.23	−0.02	1.78	1.82	−0.04
12G	4.06	4.06	0.00	2.47	2.49	−0.02	2.25	2.26	−0.01
13C	3.95	3.95	0.00	2.27	2.29	−0.02	1.80	1.82	−0.02
14G	4.24			2.62	2.66	−0.04	2.53	2.59	−0.06
15C	4.08	4.15	−0.07	2.31	2.40	−0.09	1.94	2.14	−0.20
16A	4.33	4.30	0.03	2.78	2.66	0.12	2.64	2.66	−0.02
17U	4.11			2.35			1.97	4.19	
18U	4.08			2.44			2.00	4.43	
19A	4.03			2.68			2.55	4.41	
20U	4.02			2.21			1.82	4.27	
21A	4.02	4.10	−0.08	2.74	2.59	0.15	2.57	2.29	0.28
22A	4.30	4.34	−0.04	2.65	2.72	−0.07	2.43	2.45	−0.02
23C	3.98	4.02	−0.04	2.12	2.17	−0.05	1.66	1.76	−0.10
24G		4.05		2.43	2.45	−0.02	2.23	2.24	−0.01

[a] Values in the Δ column indicate differences in chemical shift for the chimera compared to pure DNA.

H2′ region of the COSY spectra, no H1′–H2′ scalar coupling is observed for the RNA residues except the first ribonucleotide following the 3′-end of DNA (Figure 6 and the supplementary material). Both observations strongly suggest a H1′–H2′ dihedral angle close to 90°, which is a characteristic of the A-type C3′-endo conformation but not the B-type C2′-endo conformation. (3) Nonexchangeable proton chemical shift comparisons between RNA, DNA, and chimeric dodecamers of the same sequence clearly indicate an A-form conformation for the central RNA nucleotides. In our previous papers (Chou et al., 1989a,b), we established a preliminary set of chemical shift rules for the A versus B conformations, namely, in the A conformation the H8 protons of the purines move upfield, the H6 protons of the pyrimidines move downfield, and all H1′ protons move upfield compared to the B conformation. In Tables I, II, and III, all the base and H1′ protons in the central RNA segment follow these B to A shift rules; while the magnitude of the shift might vary depending on the sequence, the direction of the change obeys these rules very well.

While most of the NOEs at the junction region have different intensities compared to those of the DNA or RNA segments, the detailed structure around this region cannot be deduced from the present qualitative NOE data. A further complication is the discovery of longer T_1 values for protons in the RNA blocks (Wang et al., submitted for publication), and it will be necessary to collect 2D NOE data with much longer relaxation delays for the quantitative NOE volumes and proton distances required for accurate distance geometry studies. Such experiments are in progress.

We have also studied the circular dichroism (CD) behavior of these d-r-d chimeras and compared them to the CD spectra of the pure DNA and pure RNA sequences (data to be published). The absorption amplitudes and wavelength maxima of the chimeras appear to be the proportional summation of

the pure DNA and pure RNA spectra, which is further evidence that A-type and B-type conformations coexist in these short d–r–d duplexes.

From relatively low-resolution homopolymer 1D NMR data on dG_n:$rC_{11}dC_{16}$, Selsing et al. (1978) proposed an A–B junction model based on A-form and B-form coordinates from fiber diffraction data (Arnott & Hukins, 1972) and the assumption of optimized base stacking of the junction base pairs. By adjusting the 20 torsion angles of the two sugar–phosphate backbones linking the two junction base pairs, and with a linked-atom least-squares method to minimize steric compression, they proposed that the DNA junction base pair is heteronomous, having one residue in the C2′-endo conformation with the complementary residue in the C3′-endo conformation; this introduces a bend angle of about 20° between the A and B helix axes (Selsing et al., 1979). The conformation of the dG:rC section of their duplex is not clear, but we nevertheless find some similarities to their model in our 2D NMR data. We observe normal hydrogen-bonded complementary base pairing for the DNA and RNA base pairs at the junction. The DNA base pair at the junction is heteronomous, in that the two complementary nucleotides have different conformations; residue 9 following the last ribonucleotide appears to be in normal DNA C2′-endo-type conformation, but its complement, residue 4 preceding the first ribonucleotide, appears not to be pure C3′-endo as they propose, but rather some intermediate conformation that is neither N nor S, as evidenced by strong H1′–H2′ coupling and by the different behavior of 4G in both rAAUU and rUAUA and of 4T/16A in rAUAA compared to the other deoxyribonucleotides. The RNA base pair at the DNA–RNA interface is also heteronomous in that the first ribonucleotide of the RNA block exhibits 1′H–2′H *J* coupling while its complement does not. Thus the structural perturbation at the junction is spread over at least two base pairs. We have no definitive evidence that bending occurs at the junction region, and further studies are needed to investigate this point.

A separate NMR study of the hexamer d(CG)r(CG)d(CG) has also been reported (Haasnoot et al., 1983), but structural details of the junction conformation were lacking. These authors also suggested C3′-endo and C2′-endo heteronomous conformations for the junction base pair, but on the opposite strands to the model proposed by Selsing et al. (1979). We feel that this chimeric hexamer may be too short to reflect the true junction conformation since all of the residues in the dinucleotide RNA block occur at junctions with extremely short DNA blocks at duplex termini and would be affected on both sides by the helix-distorting junction phenomena we have demonstrated, as well as by terminal fraying effects.

Supplementary Material Available

Figures 8–11 showing 1D imino NOEs, temperature studies on imino protons of rAAUU and dAAUU, and COSY spectra of rAAUU and rUAUA. Figures 12–14 showing the NOESY spectrum of rAUAA, as well as expansions of the H8/H6 to RNA H2′/DNA H3′ and the H8/H6 to DNA H2′/H2″ regions (8 pages). Ordering information is given on any current masthead page.

Registry No. rAAUU, 133374-04-6; rUAUA, 133399-37-8; rAUAA, 133399-41-4; d(CGCGAAUUCGCG), 133399-38-9; d(CGCGUAUACGCG), 133374-05-7; d(CGTTAUAATGCG)·d(CGCAUUAUAACG), 133374-08-0.

References

Aboul-ela, F., Varani, G., & Tinoco, I. (1988) *Nucleic Acids Res. 16*, 3559–3572.

Adam, S., Ridoux, J. P., Bourtayre, P., Taillandier, E., Pochet, S., Huynh-Dinh, T., & Igolen, J. (1988) *J. Biomol. Struct. Dyn. 6*, 167–179.

Arnott, S., & Hukins, W. L. (1972) *Biochem. Biophys. Res. Commun. 47*, 1504–1509.

Arnott, S., Chandrasekaran, R., Birdsall, D. L., Leslie, A. G. W., & Ratliff, R. L. (1980) *Nature 283*, 743–745.

Arnott, S., Chandrasekaran, R., Hall, I. H., Puigjaner, L. C., Walker, J. K., & Wang, M. (1983) *Cold Spring Harbor Symp. Quant. Biol. 47*, 53–65.

Arnott, S., Chandrasekaran, R., Millane, R. P., & Park, H.-S. (1986) *J. Mol. Biol. 188*, 631–640.

Broyde, S. B., Stellman, S. D., & Wartell, R. M. (1975) *Biopolymers 14*, 2625–2637.

Chou, S. H., Hare, D. R., Wemmer, D. E., & Reid, B. R. (1983) *Biochemistry 22*, 3037–3041.

Chou, S. H., Wemmer, E. E., Hare, D. R., & Reid, B. R. (1984) *Biochemistry 23*, 2257–2262.

Chou, S. H.; Flynn, P., & Reid, B. R. (1989a) *Biochemistry 28*, 2422–2435.

Chou, S. H., Flynn, P., & Reid, B. R. (1989b) *Biochemistry 28*, 2435–2443.

Drew, H. R., Wing, R. M., Takano, T., Broka, C., Tanaka, S., Itakura, K., & Dickerson, R. E. (1981) *Proc. Natl. Acad. Sci. U.S.A. 78*, 2179–2183.

Feigon, J., Leupin, W., Denny, W. A., & Kearns, D. R. (1983) *Biochemistry 22*, 5943–5951.

Franklin, R., & Gosling, R. G. (1953) *Nature 171*, 740–742.

Haasnoot, C. A. G., Westerink, H. P., van der Marel, G. A., & van Boom, J. H. (1984) *J. Biomol. Struct. Dyn. 2*, 345–360.

Haran, T. T., Shakked, Z., Wang, A. H.-J., & Rich, A. (1987) *J. Biomol. Struct. Dyn. 5*, 199–217.

Hare, D. R., & Reid, B. R. (1986) *Biochemistry 23*, 5341–5350.

Hare, D. R., Wemmer, D. E., Chou, S. H., Drobny, G., & Reid, B. R. (1983) *J. Mol. Biol. 171*, 319–336.

Leith, I. R., Hay, R. T., & Russell, W. C. (1988) *Nucleic Acid Res. 16*, 8277–8289.

McCall, M., Brown, T., & Kennard, O. (1985) *J. Mol. Biol. 183*, 385–396.

Nelson, H. C. M., Finch, J. T., Luisi, B. F., & Klug, A. (1987) *Nature 330*, 221–226.

Nerdal, W., Hare, D. R., & Reid, B. R. (1988) *J. Mol. Biol. 201*, 717–739.

Ogilvie, K. K., Usman, N., Nicoghosian, K., & Cedergren, R. J. (1988) *Proc. Natl. Acad. Sci. U.S.A. 85*, 5764–5768.

Peticolas, W. L., Wang, Y., & Thomas, G. A. (1988) *Proc. Natl. Acad. Sci. U.S.A. 85*, 2579–2583.

Reid, B. R. (1987) *Q. Rev. Biophys. 20*, 1–34.

Reid, D. G., Salisbury, S. A., Bellard, S., Shakked, Z., & Williams, D. H. (1983) *Biochemistry 22*, 2019–2025.

Rhodes, D., & Klug, A. (1986) *Cell 46*, 123–132.

Rich, A., Nordheim, A., & Wang, A. H.-J. (1984) *Annu. Rev. Biochem. 53*, 791–846.

Scheek, R. M., Russo, N., Boelens, R., & Kaptein, R. (1983) *J. Am. Chem. Soc. 105*, 2914–2919.

Selsing, E., Wells, R. D., Early, T. A., & Kearns, D. R. (1978) *Nature 275*, 249–250.

Selsing, E., Wells, R. D., Alden, C. J., & Arnott, S. (1979) *J. Biol. Chem. 254*, 5417–5422.

Shakked, Z., Rabinovich, D., Kennard, O., Cruse, W. B. T., Salisbury, S. A., & Viswamitra, M. A. (1983) *J. Mol. Biol. 166*, 183–201.

Sheardy, R. D. (1988) *Nucleic Acids Res. 16*, 1153–1167.

States, D. J., Haberkorn, R. A., & Ruben, D. J. (1982) *J. Magn. Reson. 48*, 286.
Wang, A. H.-J., Quigley, G. J., Kolpak, F. J., van der Marel, G., van Boom, J. H., & Rich, A. (1981) *Science 211*, 171–174.
Wang, A. H.-J., Fujii, S., van Boom, J. H., van der Marel, G. A., van Boeckel, S. A. A., & Rich, A. (1982) *Nature 299*, 601–604.
Wang, Y., Thomas, G. A., & Peticolas, W. L. (1987) *J. Biomol. Struct. Dyn. 5*, 249–274.
Wemmer, D. E., Chou, S. H., & Reid, B. R. (1984a) *J. Mol. Biol. 180*, 41–60.
Wemmer, D. E., Chou, S. H., Hare, D. R., & Reid, B. R. (1984b) *Biochemistry 23*, 2262–2268.
Zimmerman, S. B., & Pheiffer, B. H. (1981) *Proc. Natl. Acad. Sci. U.S.A. 78*, 78–82.

The Z–Z Junction: The Boundary between Two Out-of-Phase Z-DNA Regions†

Brian H. Johnston,*,‡,∥ Gary J. Quigley,§,∥ Michael J. Ellison,∥,⊥ and Alexander Rich∥

Molecular Biology Department, SRI International, 333 Ravenswood Avenue, Menlo Park, California 94025, Department of Chemistry, Hunter College, City University of New York, New York, New York 10021, Department of Biochemistry, University of Alberta, Edmonton, Alberta, Canada T6A2H7, and Department of Biology, Massachusetts Institute of Technology, Cambridge, Massachusetts 02139

Received December 19, 1990; Revised Manuscript Received February 25, 1991

ABSTRACT: The boundary between two segments of Z-DNA that differ in the phase of their syn–anti alternation about the glycosidic bond is termed a Z–Z junction. Using chemical probes and two-dimensional gel electrophoresis, we examined a Z–Z junction consisting of the sequence d[$(CG)_8C(CG)_8$] inserted into a plasmid and used energy minimization techniques to devise a three-dimensional model that is consistent with the available data. We show that both alternating CG segments undergo the B–Z transiton together to form a Z–Z junction. The junction is very compact, displaying a distinctive reactivity signature at the two base pairs at the junction. In particular, the 5′ cytosine of the CC dinucleotide at the junction is hyperreactive toward hydroxylamine, and the two guanines of the GG dinucleotide on the complementary strand are less reactive toward diethyl pyrocarbonate than are the surrounding Z-DNA guanines. Statistical mechanical treatment of the 2-D gel data yields a ΔG for forming the Z–Z junction equal to 3.5 kcal, significantly less than the cost of a B–Z junction and approximately equal to the cost of a base out of alternation (i.e., a Z-DNA pyrimidine in the syn conformation). The computer-generated model shows little distortion of the Z helix outside of the central two base pairs, and the energy of the structure and the steric accessibility of the reactive groups are consistent with the data.

Z-DNA is a left-handed conformation of the double helix, characterized by a dinucleotide repeat in which anti and syn conformations of the bases alternate in succession along the chain [for review, see Rich et al. (1984)]. Because purine residues adopt the syn conformation more easily than do pyrimidine residues, Z-DNA forms most readily in sequences having alternations of purines and pyrimidines (APP sequences). Those APP sequences that most easily form Z-DNA, alternating cytosine and guanine residues [$d(CG)_n$], have been intensively studied, but long sequences of this type have not been found in natural DNA. On the other hand, long stretches of $d(CA)_n$·$d(GT)_n$ ($n \approx 15$–30) are found scattered throughout the eukaryotic genome, about once every 50–100 kb, as a form of middle repetitive DNA (Hamada et al., 1982). In addition, long APP tracts having mixed sequence have identified in many sites, including regulatory regions, in various genomes. All the above sequences can be shown to form Z-DNA in vitro under negative superhelical tension (Rich et al. 1984). [Of the simple APP sequences, only $d(AT)_n$ appears not to readily form Z-DNA (Ellison et al., 1986).] Although the biological role of Z-DNA is not well understood, there is evidence that Z-DNA forms in vivo in *Escherichia coli* (Haniford & Pulleyblank, 1983; Jawarsky et al., 1987; Rahmouni & Wells, 1989) as well as in eukaryotic nuclei capable of carrying out replication and transcription (Wittig et al., 1989).

In addition to strictly alternating purine–pyrimidine sequences, natural DNA contains many examples of alternating sequences in which the phase of alternation changes in the midst of the sequence. If such a sequence is in the Z conformation, a Z–Z junction will exist at the change in phase. For example, the sequence 5′-$(CG)_n(GC)_n$-3′ could form Z-DNA in each of the segments within parentheses but their phasing would be different. Thus, if the cytosines are maintained in the anti conformation and the guanines in the syn conformation, the sequence of conformations at the center of the sequence (...CGCGGCGC...) on one strand would be anti-syn-anti-syn-syn-anti-syn-anti (syn-anti-syn-anti-anti-syn-anti-syn on the other strand). It is the two adjacent syn

†Supported by NIH Postdoctoral Fellowship 3F32GM09031 and NIH Grant 1R29GM41423 to B.H.J.; NIH Grant GM41359, PSC-CUNY Grant 668255 and NIH Research Centers in Minority Institutions Award RR-03037 to G.J.Q.; and grants from the NIH, the NSF, the Office of Naval Research, NASA, and the American Cancer Society to A.R. M.J.E. was supported by a postdoctoral fellowship from the Medical Research Council of Canada. This work was first presented at the Fifth Conversation in Biomolecular Stereodynamics, Albany, NY, 1987.

* To whom correspondence should be addressed at SRI International.
‡ SRI International.
∥ Massachusetts Institute of Technology.
§ City University of New York.
⊥ University of Alberta.

0006-2960/91/0430-5257$02.50/0